A MONOCULAR OCCUPANCY GRID FOR LOCAL WMR NAVIGATION

Lluís Pacheco, Xavier Cufí
Technical School, Girona University, Av. Luís Santaló s/n, Girona, Spain

Ningsu Luo, Javier Cobos
Institut de Informàtica i Aplicacions, Girona University, Av. Lluís Santaló s/n, Girona, Spain

Keywords: Autonomous mobile robots, Computer vision, Path planning, Obstacle avoidance, Reactive navigation.

Abstract: This work introduces a new methodology to infer environment structure by using monocular techniques. The monocular field of view is constrained to the vicinity of the mobile robot. The cooperative strategy proposed combines DFF and qualitative structure techniques to obtain environment information. The remarkable features of the strategy presented are its simplicity and the low computational cost. In this way, a simplified DFF method, which uses only one frame, has been implemented; hence, scenario information can be achieved when homogeneous radiance background constraint is accomplished. Further structure analysis is developed by computing qualitative structure through time integration series of acquired frames; within a tessellated probabilistic representation consisting in a local occupancy grid framework. Furthermore, the camera pose knowledge is used to correlate the different overlapping image zones. Moreover, time integration of the monocular frames allows a larger environment description suitable for WMR local path planning. Hence, the reported work can be used in obstacle avoidance strategies or reactive behaviours for navigation towards the desired objective.

1 INTRODUCTION

Perception of the environment is based on the sensor system measurements that provide distances and structure knowledge. This essential task could be accomplished by different range systems like ultrasonic sensors, laser rangefinders, or vision based systems. All these sensors have their advantages and disadvantages. However, computer vision based methods, are one of the most attractive. Therefore, they have many interesting advantages that can be summarized as follows: the falling prices of devices and richer information compared with the other traditional ranging devices. In this way the increasing capabilities of the personal computers, offer an interesting range of real time applications. Perception systems based on camera devices have attracted robotic research due these interesting features. Thus, machine vision systems have used some features of eyes, such as stereopsis, optical flow or accommodation, as meaningful clues. SVS (stereo vision systems), OFM (optical flow methods) and DFF (depth from focus) are all methods that permit 3D scene recovery. Studies comparing SVS and DFF are reported in (Schechner and Kiryati, 1998). The results show that while SVS has greater resolution and sensitivity, DFF has greater robustness, requires less computational effort and can deal properly with correspondence and occlusion problems. The need for several images of the same scene, acquired with different optical setups, may be considered as a significant drawback in using DFF methods in major robotic applications. The scientific community has proposed the use of special cameras, such as a multi-focus camera that acquires three images with three different focus positions (Hiura and Matsuyama, 1998). However, other proposals were developed due to a lack of multi-focus commercial cameras. The use of DFF in WMR (wheeled mobile robots) has been reported in (Nourbakhsh, 1997); in which Noubakhsh used three cameras with almost the same scene to achieve robust and efficient obstacle detection.

This work presents a new cooperative monocular strategy; where DFF and QSM (Qualitative

Pacheco L., Cufí X., Luo N. and Cobos J. (2009).
A MONOCULAR OCCUPANCY GRID FOR LOCAL WMR NAVIGATION.
In *Proceedings of the 6th International Conference on Informatics in Control, Automation and Robotics - Robotics and Automation*, pages 425-432
DOI: 10.5220/0002206704250432

Structure Methods) are combined. Thus, one bit depth can be obtained using the DFF methodology as well as a set of multi-resolution focus thresholds, when homogeneous radiance background constraint is accomplished. However, when homogeneous radiance constraint fails, we propose to use QSM over discrepancy areas in order to infer environment structure by using an occupancy grid framework. Therefore, the main contributions of this research are to propose the occupancy grid as a suitable structure in order to infer qualitative obstacle structure and obtaining larger scenario descriptions. The results depicted are directed towards real applications by using the WMR PRIM, which consists of a differential driven one with a free rotating wheel (Pacheco et al., 2008). The experiments are orientated so as to obtain a local map in the robot's neighborhood that can be used to plan navigation strategies.

This paper is organized as follows. In Section 1, the main ideas and research objectives are presented. Section 2 introduces the DFF methodology as well as the algorithms and results implemented. Section 3 depicts the QSM concept and the related algorithms used. In this way, the local occupancy grid framework is also formulated as a way for time integrating the acquired frames. In Section 4, the experimental preliminary results are drawn by using the mobile platform PRIM. In Section 5 the conclusions and future research are presented.

2 THE CONSTRAINED DFF SYSTEM DESCRIPTION

This section briefly introduces the DFF methodology. The algorithms implemented as well as their results are also depicted by using the available WMR platform. Its significant contribution is the use of a single image to obtain environment information.

The DFF techniques use an image collection of the same scene acquired at different focus positions. Thus, the camera system PSF (point spread function) for unfocused object points produces blurred image points. The PSF frequency domain space transform representations arise in a first order Bessel OTF (optical transfer function), where its main lobe volume can determine the FM (focus measure) expressed as:

$$M_0 = \iint \left| I_i(\omega,\nu) \right| d\omega d\nu \,. \qquad (1)$$

where I_i denotes the image considered, ω and ν represent the frequency components. Efficient energy image measures have been proposed as FM (Subbarao et al, 1992). Nayar has proposed a modified Laplacian that improves the results in some textures (Nayar and Nakagawa, 1994). The 3D scene map and passive auto-focus consumer camera systems are interesting applications solved by the DFF. Recovering the 3D information from DFF methods is known as SFF (shape from focus) (Nayar and Nakagawa, 1994).

2.1 The DFF Monocular Algorithms

The algorithms of the machine vision system implemented are based on important assumptions that are generally obtained in normal indoor scenarios, but also in many outdoor scenarios. These constraints are flat and homogenous energy radiance from the floor surface and experimental knowledge of the focus measurement threshold values. Two important aspects, image window size and camera pose, should be considered. The size of windows should be big enough to receive energy information. For example, in the work of Surya, images of 150x150 pixels were used, and the focus measures were computed in 15x15 pixel regions (Surya, 1994). The camera pose will set the scenario perspective and consequently the floor position coordinates that should be used in the WMR navigation strategy. Figure 1 shows the robot and camera configuration considered in this work, where α, β and φ are angles of the vertical and horizontal field of view and the tilt camera pose respectively. The vertical coordinate of the camera is represented by *H*. The robot coordinates corresponding to each pixel can be computed using trigonometric relationships and the corresponding knowledge of the camera configuration (Horn, 1998). Using trigonometric relationships, the flat floor scene coordinates can be computed as follows:

$$\begin{aligned} X_{i,j} &= \pm \frac{H}{\cos(\varphi - \alpha/2 + \Delta\alpha)} \tan(\Delta\beta) \\ Y_j &= H \tan(\varphi - \alpha/2 + \Delta\alpha) \\ \Delta\beta &= K_i \frac{\beta}{C} \qquad (0 \le K_i \le C/2) \\ \Delta\alpha &= K_j \frac{\alpha}{R} \quad (0 \le K_j \le R) \end{aligned} \qquad (2)$$

K_i and K_j are parameters used for covering the discrete space of the image pixels. Thus, *R* and *C* represent the image resolution through the total number of rows and columns. It should be noted that for each row position corresponding to scene

coordinates Y_j, there are C column coordinates $X_{i,j}$. The above equations provide the available local map coordinates when no obstacle is detected. The algorithms used are explained in the remainder of this subsection. The multigrid representation using low-pass filtering processes can improve the surface radiance homogeneity. Scale space representations can reduce the search space, increasing the computation performance (Gonzalez and Woods, 2002). Therefore, a Gaussian filter is applied to the frames acquired in PAL format, at 768x576 pixels. Three decreasing resolution levels have been used with picture sizes of 384x288, 192x144 and 96x72. The average image brightness is also computed. In order to achieve greater robustness against changes in lightness, brightness normalization is performed (Surya, 1994). The image energy is computed, over 3x3 windows at the top level of the scale-space, using the modified Laplacian method:

$$ML(x,y) = |2i(x,y) - i(x-1,y) - i(x+1)| + |2i(x,y) - i(x,y-1) - i(x,y+1)| \quad (3)$$

where $i(x,y)$ represents the corresponding pixel value at spatial coordinates (x,y). The 96x72 scale-space is decreased using a 9x7x2 array, where each cell represents the Laplacian mean value and the corresponding standard deviation mean computed over 10x10 pixel patches. Another interesting statistical parameter that has been used is the standard deviation, which relates to the homogeneity of the floor energy values. The 9x7x2 array is explored, from top to bottom; floor segmentation is carried out, using both energy and standard deviation thresholds.

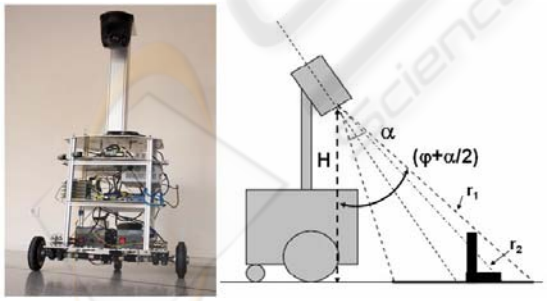

Figure 1: The robot PRIM and the monocular camera configuration. Where α is set to 37º, β (horizontal angle) of 48º, H set to 109cm, and a tilt angle of 32º.

2.2 One Bit DFF Experimental Results

The floor threshold has been experimentally computed by averaging several floor images acquired in our lab environment with different kinds of illumination (from 200-2000 lx). Light illumination can change from 2000 lx when light from the sun is clearly present where there is sunlight through the windows, to less than 200 lx in the darker corridor zones. Figure 2 depicts high resolution (130x130 pixel windows) corresponding to different floor images used to compute focus measurement thresholds where the floor texture is clearly visible. It is in the locality of those points where the information about radiance is obtained. Hence, the results obtained with the available experimental set up show the decreasing values when the distance between the camera and the floor is increased. A more complete description of the energy floor radiance measures obtained for each 9x7 visual perception row is shown in (Pacheco et al., 2007); in which the image perspective emerges from a set of multi-resolution thresholds as a function of the camera distances.

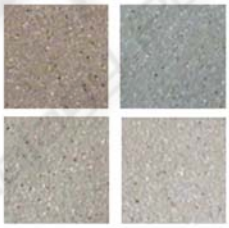

Figure 2: Fragments of high resolution floor images (768x576 pixels under different light conditions corresponding to 300, 800, 1400 and 2000 lx, respectively.

Figure 3 shows the modified Laplacian energy and standard deviation values using 9x7 and 96x72 space-resolutions, when typical indoor obstacles are presented. It is shown that 9x7 space resolutions can detect radiance discontinuities but because there was

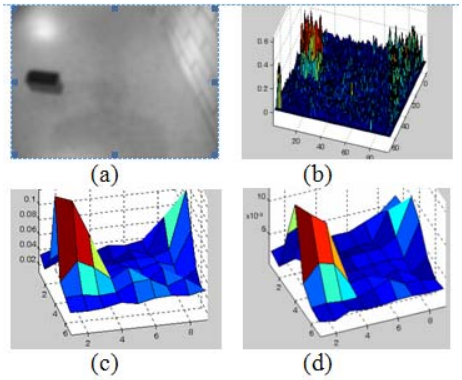

Figure 3: (a) Image with obstacles, 96x72; (b) Modified Laplacian measures; (c) 9x7 Modified Laplacian mean values; (d)) 9x7 standard deviation mean.

a great lack of resolution manifested through soft slopes. Thus, it is necessary to use a fine space-resolution to attain the sharper edges. In this work, 9x7 resolutions are used to detect the local patches where obstacle segmentation is computed within 96x72 space resolution.

Despite the good results achieved, some further improvements should be considered. Hence, when radiance floor discontinuites occur they can be considered obstacles (false positives in some cases). Therefore in next section OFM is introduced, within the occupancy grid framework, to improve the one bit DFF methodology.

3 QUALITATIVE STRUCTURE METODS AND OCCUPACY GRID

The camera pose and local field of view will set the QSM algorithms reported in this section. The different optical flow quantitative approaches are generally based on two classical feasible assumptions, which are BCM (brightness constancy model), and optical flow smoothness. Thus, image motion discontinuities are due to the depth and motion discontinuity boundaries. Hence, there are places where image flow changes are suddenly useful as image segmentation clues, but can cause problems such as optical flow estimation clusters. Therefore, suggestions made to compute the algorithms over small neighborhoods, or region-based matched methods have turn on. Combining local and global optic flow differential methods have been proposed as a way to share benefits from the complementary advantages and short-comings (Bruhn, 2002).

The occupancy field can be depicted by a probability density function that relates sensor measures to the real cell state. The tessellated probabilistic representation has been widely adopted by the scientific community in navigation or mapping issues. Indoor applications research has been mainly concentrated on SLAM (simultaneous localization and mapping) issues (Thrun, 2002). Their use allows sensor fusion or multiple layer representations to segment dynamic objects (Coue, 2006). The perception system used, in this work, consists in monocular and odometer system data. The use of these systems in SLAM is reported in (Cumani et al., 2004).

The main difference of the research depicted in this paper, as compared with Cumani research, is the occupancy grid use that allows integration of multiples frames without constraining their number. Furthermore, it is obtained a local map description suitable for navigation. Thus, the occupancy grid developed research increase the camera narrow field of view, which provides just the vicinity of the robot where floor only is expected to be found. Moreover, the floor model is also proposed as a contribution in order to build the 2D occupancy grid; hence obstacle binary results are time integrated within the local occupancy grid framework by considering such model. The obstacle structure could be inferred by considering optical flow magnification change discrepancies from the floor model.

3.1 The Local QSM Approach

In the present research the camera field of view depicts only the vicinity of the WMR. Perspective projection, as shown in Figure 4, should be assumed.

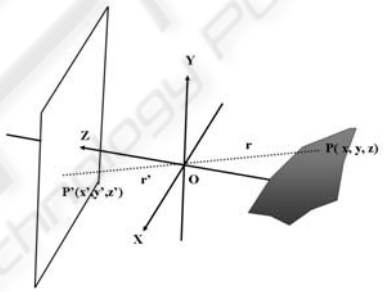

Figure 4: Camera system producing an image that is a perspective projection of the world.

Introducing the coordinate system, where z coordinates are aligned to the optical camera, and the xy-plane is parallel to the image plane, the image P' corresponding to the point P of a scene object is given by the following expressions:

$$\begin{aligned} &\frac{x'}{z'}=\frac{x}{z} \quad \frac{y'}{z'}=\frac{y}{z} \qquad -z = r\cos\alpha \\ &\Rightarrow r = -\frac{z}{\cos\alpha} = -z\sec\alpha \\ &z' = r'\cos\alpha \Rightarrow r' = \frac{z'}{\cos\alpha} = z'\sec\alpha \end{aligned} \tag{4}$$

Where z' in the distance between image plane and the camera lenses, and x' and y' are the image coordinates. The object point coordinates, referred to the optic center O, are given by $P= (X, Y, Z)$, being r de distance between P and O and α the angle. The ratio of the distance between two points measured in the image plane and the corresponding points measured in the scene is called magnification m.

$$m = \frac{\sqrt{(\Delta' x)^2 + (\Delta' y)^2}}{\sqrt{(\Delta x)^2 + (\Delta y)^2}} = \frac{z'}{z} \quad (5)$$

For reduced field of views when the optical rays are parallel to the optical axis the magnification *m* is constant for all the image points. However, due to the field of view and camera pose assumed in this research, magnification changes are expected even when just considering a flat floor scenario. Hence, the perspective image formation model arises in magnification changes. Figure 5 shows the magnification changes of the floor model by considering the optical axis ray as the unit of magnification. Therefore, these changes in magnification are made it more complicated to look for image patches with similar motion in order to detect obstacle depth boundaries. However, by using the floor model and the odometer system data, binary floor results can be predicted from frame to frame; then predicted discontinuities arise due to the 3D non floor obstacle shapes that produce unexpected image boundaries.

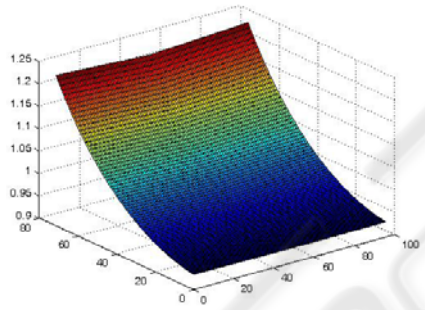

Figure 5: Magnification changes of the floor model by considering the optical axis ray as the unit of magnification**.** The bigger magnification is attained at closer robot positions.

The machine vision system algorithms implemented are based on binary results obtained by the one bit DFF algorithms explained in subsection 2.2. Binary images are obtained in the 96x72 space resolution level, and blob analysis is developed. The blob areas and the extremes of their coordinates are computed and small blobs are removed. Then, the image is analyzed from top to bottom, searching for possible non floor regions. Hence, the QSM can be used to detect the possible obstacles, when important floor energy radiance discrepancies are met. Therefore, using relative robot coordinate increments provided by the odometer system, qualitative structure estimation could be done by comparing predicted positions with the binary results obtained. The time integration of the different frames acquired is introduced in the next section. Thus, the robot coherent interaction with the world can be addressed by using the occupancy grid framework that provides a robust and unified approach to a variety of problems in spatial robot perception and navigation (Elfes, 1989).

3.2 The Local Occupancy Grid Framework

The occupancy grid is considered to be a discrete stochastic process defined over a set of continuous spatial coordinates *(x, y)*. Hence, the space is divided into a finite number of cells representing a 2D position, $1 \le j \le R$ $1 \le i \le C$. The *R* and *C* parameters are the number of rows and columns of the grid respectively. The cell column coordinates are designated by X_i and the rows by Y_j. It is assumed that local occupancy grid data is provided by the on-robot perception system. The occupancy probability is divided into two ranges only: free and occupied. The grid can be updated by using the sensor models and the current information. Hence, given a sensor measurement *m*, the occupancy probability *P(O)* for the different cells, $P(C_{ij})$, can be computed by applying Bayes rule:

$$P(O|C_{ij}) = \frac{P(C_{ij}|O)}{P(C_{ij}|O) + P(C_{ij}|/O)} \quad (6)$$

Hence, the probability that a cell is occupied $P(O/C_{ij})$ is given by the cell occupancy sensor measurement statistics $P(C_{ij}/O)$ by also considering the probability that the cell will be free $P(C_{ij}//O)$. Thus, free cells have binary results equal to zero; these non-occupied cells belong to coordinates for image pixels within floor radiance thresholds. Other available coordinates are provided through time integration of the acquired frames when radiance energy is bigger than threshold values, by using the floor model, and looking for coincidences with the acquired frames. The unknown probability value is set to 0.5. Therefore, by using the expression (6) with the predicted occupied cells and acquired frames, the grid positions belonging to the floor will provide larger occupancy values. Obstacle positions give intermediate occupancy probabilities due to the discrepancies between the predicted and the acquired image values that arise due to the 3D obstacle shape. Next section depicts some preliminary results experimented with the available WMR platform.

(a) (b) (c)

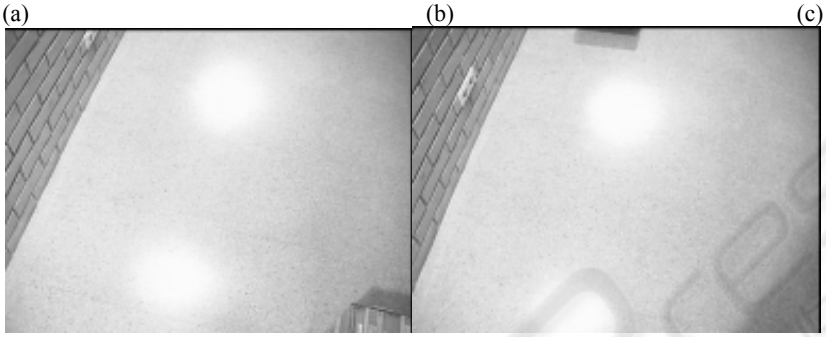

(d) (e)

Figure 8.a, 8.b, 8.c, 8.d, and 8.e: It is depicted the monocular frames acquired while the WMR is avoiding the first obstacle placed on the direction towards the objective.

4 ON-ROBOT EXPERIENCES

In this section are presented some experimental results using the WMR PRIM. Thus, local navigation with static obstacles is used as a preliminary test of the research introduced in this paper. The navigation and control strategy used, under this reduced field of view, is introduced in other author's work (Pacheco and Luo, 2007). Therefore, the maximum geometric size of the closer obstacle is considered in order to plan safety navigation towards the desired coordinates.

Figure 6: It is presented the real scenario that has been drawn in Figure 7. It is shown the obstacles placed on the floor that the WMR should avoid.

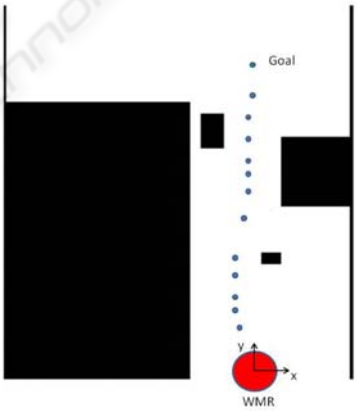

Figure 7: Simplified map scenario where the robot trajectory toward the goal is depicted with blue dots. The obstacles are drawn in black.

Figure 6 shows the scenario where the experiment has been done, and Figure 7 depicts the simplified map scenario with the WMR achieved trajectory.

Thus, Figure 7 shows the lab environment map and the path followed when the WMR starts at the position (0, 0, 90º) towards the desired coordinates (0, 460cm). The scenario contains some static obstacles that the WMR should avoid.

Table 1 depicts the robot coordinates and acquired frames during the WMR navigation.

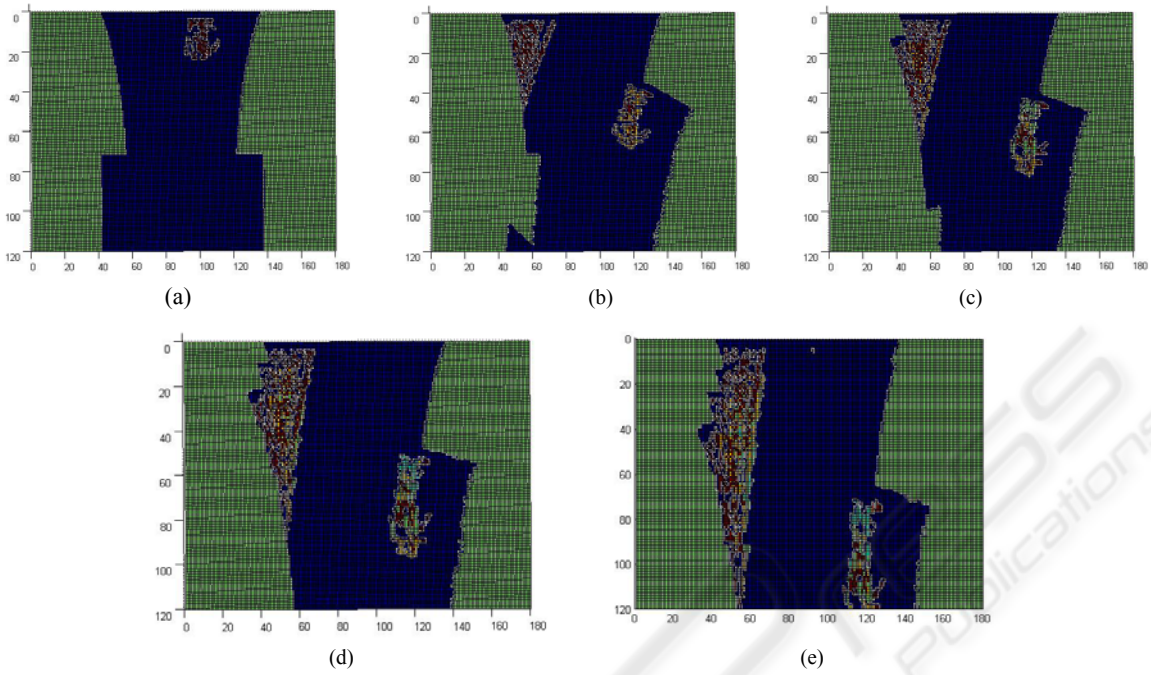

Figure 9: Sequence of occupancy grids obtained by integrating the first 5 acquired frames.

Table 1: Coordinates from where the frames are acquired.

F.1	(0, 0, 90º)	F.7	(1, 293, 76º)
F.2	(-11, 66, 110º)	F.8	(4, 315, 88º)
F.3	(-21, 108, 99º)	F.9	(4, 339, 96º)
F.4	(-25, 141, 97º)	F.10	(6, 375, 89º)
F.5	(-26, 176, 94º)	F.11	(4, 415, 100º)
F. 6	(-8, 248, 83º)	F.12	(12, 456, 74º)

The first 5 frames are acquired during the obstacle avoidance strategy of the first obstacle placed in the middle of the corridor. Figure 8.a, 8.b, 8.c, and 8.d. show these frames.

The first obstacle avoidance strategy consists into turn to the left in order to avoid the collision with the obstacle that appears at the first four frames. It is noted that fifth frame, Figure 8.e, depicts a part of the scenario where doesn't appear the first obstacleThe local occupancy grid built by integrating the first 5 frames is shown in Figure 9.a, 9.b, 9.c, 9.d, and 9.e. It is depicted that in the first frame only the front obstacle is perceived. However, when the other frames are integrated the left wall is integrated. It is observed how the WMR navigation is constrained by the different obstacles obtained on the acquired frames and integrated within the occupancy grid. Therefore the navigation is constrained by both obstacles. Moreover the fifth frame is integrated in Figure 9.e where appear as time integrated the front obstacle and the left wall. Hence, the monocular occupancy grid methodology presented increases the field of view perception, and a better navigation strategy can be planned. The integration of multiple monocular frames also can be used as a framework in order to infer 3D obstacle structure.

5 CONCLUSIONS

The methodology presented in this research has provided a local map suitable for WMR navigation. Therefore a short-term memory has been obtained. Navigation advantages by using short-term memory were reported in previous research (Schäfer et al., 07). However, experimental results conducted to obtain the obstacle structure have some aspects that should focus the future work. The obstacle shape is larger than the real shape due to the magnification changes that arise of perspective. The lack of accuracy increases the path-width, and consequently this can result in larger trajectories or even infeasible path perceptions where available paths are possible. 3D obstacle structure can solve the above problem. But, the results obtained in order to obtain 3D information have some mismatches when overlapping areas between predicted and obtained blobs are analysed. The errors can be produced by the following sources:

- Odometry errors.
- Camera calibration errors.

- Flat floor model differences.

Future work will be addressed to solve the above problems. We believe that the occupancy grid framework can be used to obtain 3D obstacle structure. Therefore, there is not limitation concerning to the number of frames that can be time-integrated. The future goal will consist in to find a set of parameters in order to infer 3D obstacle structure. These set of parameters should be independent of the source of errors pointed in this section. The knowledge of 3D structure can afford several benefits that can be summarised as follows:

- To reduce the trajectories.
- Visual Odometry.
- Landmark detection.

Despite the work that remains undone the methodology presented can be used to direct the future research. Moreover, some good features and results are presented in this work.

ACKNOWLEDGEMENTS

This work has been partially funded by the Commission of Science and Technology of Spain (CICYT) through the coordinated project DPI-2007-66796-C03-02, and by the Government of Catalonia through the Network Xartap and the consolidated research group's grant SGR2005-01008.

REFERENCES

Bruhn A., Weickert J., Schnörr C., 2002. Combining the advantages of local and global optimal flow methods, *In Proc. Pattern Recognition, Lect. Notes in Comp. Science*, Springer-Verlag, 454-462.

Coue, C., Pradalier, C., Laugier, C., Fraichard, T., Bessiere, P., 2006. Bayesian Occupancy Filtering for Multitarget Tracking: An Automotive Application. *The Inter. Journal of Robotics Research*, 25(1) 19-30.

Cumani A., Denasi S., Guiducci A., Quaglia G., 2004. Integrating Monocular Vision and Odometry for SLAM. *WSEAS Trans. on Computers*, 3(3) 625-630.

Elfes, A., 1989. Using occupancy grids for mobile robot perception and navigation. *IEEE Computer,* 22(6) 46-57 .

Gonzalez, R. C., Woods, R. E., 2002. Digital Image Processing, *Prentice Hall Int. Ed*., Second Edition.

Hiura, S., Matsuyama, T., 1998. Depth Measurement by the Multi-Focus Camera, *Proc. IEEE CVPR*, 953-959.

Horn, B. K. P., 1998. Robot Vision, McGraw-Hill Book Company, MIT Press Edition, 12th printing.

Nayar S.K., Nakagawa, Y., 1994. Shape from Focus, *IEEE Trans. PAMI*, 16(8), 824-831.

Nourbakhsh, I., Andre, D., Tomasi, C., Genesereth, M.R., 1997. Mobile Robot Obstacle Avoidance via Depth from Focus, *Robotics and Autom. Systems*, Vol. 22, 151-158.

Pacheco, L., Luo, N., 2007. Trajectory Planning with Control Horizon Based on Narrow Local Occupancy Grid Perception. *Lect. Notes in Control and Inform. Sciences 360*, Springer-Verlag, pp. 99-106.

Pacheco, L., Cufí, X., Cobos, J., 2007. Constrained Monocular Obstacle Perception with Just One Frame, *Lect. Notes in Comp. Science*, Springer-Verlag, Pattern Recog. and Image Analysis, Vol. 1, 611-619.

Pacheco, L., Luo, N., Ferrer, I., Cufí,, X., 2008. Control Education within a Multidisciplinary Summer Course on Applied Mobile Robotics, *Proc. 17th IFAC World Congress,* pp. 11660-11665.

Schäfer H., Proetzsch M., Berns K., 2007. Obstacle Detection in Mobile Outdoor Robots, *Proc. Inter. Conf. on Informatics in Control, Autom. and Robotics*, pp. 141-148.

Schechner, Y., Kiryati, N., 1998. Depth from Defocus vs. Stereo: How Different Really Are They?, *Proc. IEEE CVPR,* Vol. 2, 256-261.

Subbarao, M., Choi, T., Nikzad, A., 1992. Focusing Techniques, *Tech. Report 92.09.04*, Stony Brook, NewYork.

Surya, G., 1994. Three Dimensional Scene Recovery from Image Defocus. *PHD thesis*, Stony Brook, New York.

Thrun S., 2002. Robotic mapping: a survey. Exploring Artificial Intelligence in the New Millennium, *Morgan Kaufmann*, San Mateo.